Geophysical Research Letters

RESEARCH LETTER
10.1029/2022GL099175

Key Points:

- Aerosol mass extinction efficiency can increase up to a factor of 2–3 after 1 day of aging
- Changes in both particle mean diameter and real part of the refractive index are needed to fully explain the changes
- Changes in the estimated real part of the refractive index are correlated to organic aerosol oxidation state, volatility, and particle size

Supporting Information:

Supporting Information may be found in the online version of this article.

Correspondence to:

P. E. Saide,
saide@atmos.ucla.edu

Citation:

Saide, P. E., Thapa, L. H., Ye, X., Pagonis, D., Campuzano-Jost, P., Guo, H., et al. (2022). Understanding the evolution of smoke mass extinction efficiency using field campaign measurements. *Geophysical Research Letters*, *49*, e2022GL099175. https://doi.org/10.1029/2022GL099175

Received 15 APR 2022
Accepted 12 SEP 2022

Understanding the Evolution of Smoke Mass Extinction Efficiency Using Field Campaign Measurements

Pablo E. Saide[1,2], Laura H. Thapa[1], Xinxin Ye[1], Demetrios Pagonis[3,4], Pedro Campuzano-Jost[3,4], Hongyu Guo[3,4], Melinda L. Schuneman[3,4], Jose-Luis Jimenez[3,4], Richard Moore[5], Elizabeth Wiggins[5], Edward Winstead[5], Claire Robinson[5], Lee Thornhill[5], Kevin Sanchez[5], Nicholas L. Wagner[4,6], Adam Ahern[4,6], Joseph M. Katich[4,6], Anne E. Perring[4,7], Joshua P. Schwarz[6], Ming Lyu[4,6], Christopher D. Holmes[8], Johnathan W. Hair[5], Marta A. Fenn[5,9], and Taylor J. Shingler[5,9]

[1]Department of Atmospheric and Oceanic Sciences, University of California—Los Angeles, Los Angeles, CA, USA, [2]Institute of the Environment and Sustainability, University of California—Los Angeles, Los Angeles, CA, USA, [3]Department of Chemistry, University of Colorado Boulder, Boulder, CO, USA, [4]Cooperative Institute for Research in Environmental Sciences, University of Colorado, Boulder, Boulder, CO, USA, [5]NASA Langley Research Center, Hampton, VA, USA, [6]National Oceanic and Atmospheric Administration, Chemical Sciences Laboratory, Boulder, CO, USA, [7]Department of Chemistry, Colgate University, Hamilton, NY, USA, [8]Department of Earth, Ocean, and Atmospheric Science, Florida State University, Tallahassee, FL, USA, [9]Science Systems and Applications Inc, Hampton, VA, USA

Abstract Aerosol mass extinction efficiency (MEE) is a key aerosol property used to connect aerosol optical properties with aerosol mass concentrations. Using measurements of smoke obtained during the Fire Influence on Regional to Global Environments and Air Quality (FIREX-AQ) campaign we find that mid-visible smoke MEE can change by a factor of 2–3 between fresh smoke (<2 hr old) and one-day-old smoke. While increases in aerosol size partially explain this trend, changes in the real part of the aerosol refractive index (real(n)) are necessary to provide closure assuming Mie theory. Real(n) estimates derived from multiple days of FIREX-AQ measurements increase with age (from 1.40 – 1.45 to 1.5–1.54 from fresh to one-day-old) and are found to be positively correlated with organic aerosol oxidation state and aerosol size, and negatively correlated with smoke volatility. Future laboratory, field, and modeling studies should focus on better understanding and parameterizing these relationships to fully represent smoke aging.

Plain Language Summary A common way to observe airborne particles produced by biomass burning is through aerosol optical properties, for instance, using aerosol optical depth from satellites or low-cost sensors that measure scattered light. Since health effects are associated to aerosol mass concentrations, a conversion factor between them is needed. Here we use in-plume measurements collected from an aircraft to show that aging processes alone can produce a factor of 2–3 change in aerosol extinction per unit of aerosol mass concentration. We also find that these changes are driven not only due to changes in aerosol size, but also due to changes in the material properties of aerosols. These results are relevant as fires are becoming more common and extreme, and thus these changes in smoke properties need to be taken into consideration in many fields of study such as assimilating satellite smoke into atmospheric composition models, satellite-based smoke impacts on health, and corrections for low-cost $PM_{2.5}$ sensors.

1. Introduction

Smoke from wildfires can have a wide range of impacts, including adverse effects on human health (O'Dell et al., 2021; C. E. Reid et al., 2016), reduction in visibility (Spracklen et al., 2007), and climate implications (Randerson et al., 2006). The severity of wildfires has been predicted to increase with climate change (Jin et al., 2015; Spracklen et al., 2009), and recent wildfire seasons across the world are confirming this by being devastating by many measures (Deb et al., 2020; Higuera & Abatzoglou, 2021).

Aerosol optical properties play an important role in observing and quantifying smoke and its impacts. For instance, satellite-derived aerosol optical depth (AOD), as well as aerosol extinction and backscattering coefficient can be used to provide constraints on smoke emissions (Ichoku & Ellison, 2014; Peterson et al., 2021; Saide et al., 2015) and to estimate surface $PM_{2.5}$ when surface networks are not available (Cheeseman et al., 2020; Mirzaei et al., 2020). Also, increasingly common low-cost sensors quantify $PM_{2.5}$ by measuring light scattering (Delp & Singer, 2020), which can be useful to extend the coverage of reference networks (Forehead et al., 2020).

These examples show that, while optical properties are sampled, many times the quantity of interest is a measure of smoke mass (e.g., concentrations or emissions). Thus, a key parameter to understand is the efficiency at which a unit of aerosol mass concentration produces aerosol extinction (scattering + absorption) or scattering, generally referred to as mass extinction efficiency (MEE) and mass scattering efficiency (MSE). Laboratory and field measurements have found a large range in mid-visible MSE for fresh and aged smoke (1.5–6 m^2/g for wavelengths on the 532–550 nm range), with values being correlated with changes in aerosol mean diameter as expected from Mie theory (Kleinman et al., 2020; Laing et al., 2016; Levin et al., 2010; J. S. Reid et al., 1998; J. S. Reid, Eck, et al., 2005). Aerosol size increase with age is the result of a combination of coagulation and gas-to-particle conversion of semi-volatile material (Martins et al., 1996; J. S. Reid, Koppmann, et al., 2005), likely primarily coagulation (Hodshire et al., 2021; June et al., 2022).

The complex refractive index is an intrinsic property of the aerosols that describes how light interacts with the material in terms of the scattering (real part) and absorption (imaginary part) (Moosmüller et al., 2009), and thus also influences MEE and MSE. Numerous laboratory and field estimates of the real refractive index have been made for biomass burning. Average real refractive index in mid-visible wavelengths for ambient wildfire smoke has been found to be in the 1.52–1.55 range, while the whole range of smoke measurements tend to be within 1.42–1.61 (Aldhaif et al., 2018; Bian et al., 2020; Espinosa et al., 2017). Similar averages and ranges are found in laboratory studies (Levin et al., 2010; Sumlin et al., 2018; Womack et al., 2021). While these studies sampled a mixture of smoke ages, the evolution of refractive index and dependence on other smoke aerosol intrinsic properties was not explored. While there is a relevant body of literature studying changes of real refractive index of organic aerosol (other than smoke) with aging (Moise et al., 2015 and references therein), there is limited literature on the topic for smoke aerosols.

Here we use observations from the 2019 NOAA-NASA FIREX-AQ field campaign to assess the evolution of MEE with smoke age. FIREX-AQ occurred during a below-average (compared to recent years) fire season, which enabled tracking of individual plumes for much longer time periods and without plumes of interest mixing with smoke from other fires. In the following, we describe the observations and computational methods, analyze and discuss results, and provide future directions.

2. Materials and Methods

2.1. Observations

FIREX-AQ measurements on board the DC-8 research aircraft for western US wildfires were used in this study. Aerosol mass concentrations were obtained from a high-resolution time-of-flight aerosol mass spectrometer (AMS for short) (Guo et al., 2021 and references therein) and the NOAA Single Particle Soot Photometer (SP2, Lamb et al., 2018). AMS was also used to quantify bulk organic aerosol (OA) properties such as the oxygen to carbon (O:C) ratio (Canagaratna et al., 2015), oxidation state (OS_c), density (Kuwata et al., 2012), and volatility, the latter defined as the mass fraction remaining (MFR) of organic aerosol after a thermodenuder set at 40°C and ~70 s residence time (see details in Text S1 in Supporting Information S1).

Aerosol optical properties were measured by two teams. The NASA team measured aerosol scattering and absorption coefficients using a nephelometer (at 450, 550, and 700 nm wavelengths) and a particle soot absorption photometer (at 470, 532, and 660 nm wavelengths), respectively, which were then combined to calculate the aerosol extinction coefficient at 532 nm wavelength (Ziemba et al., 2013). The NOAA team used a cavity ringdown spectrometer (Langridge et al., 2011) to measure extinction at 532 nm wavelength. The NOAA measurements also included extinction measurements after a thermodenuder set at 250°C and 1–2 s residence time that allowed the computation of extinction fraction remaining (EFR), another proxy for aerosol volatility. All these were taken at dry conditions. Additionally, OA concentrations and NASA extinction and scattering coefficients were corrected for in-cabin evaporation of OA as described in Text S1 in Supporting Information S1.

Aerosol size distributions were measured by multiple instruments but the main one used here is the LAS (Moore et al., 2021). A second LAS measured behind a thermodenuder set at 350°C and 1–2 s residence time, which was used to compute the volume fraction remaining (VFR) as an additional metric for aerosol volatility. Additional details on these observations, on other observations, on measurement uncertainties, on smoke age estimates, and on plume identification are described in Text S1 in Supporting Information S1.

2.2. Optical Properties Calculations

For a given wavelength, MEE is defined as the dry extinction coefficient (σ_{ext}) per unit of mass concentration (M) of an aerosol population:

$$\text{MEE} = \frac{\sigma_{\text{ext}}}{M} \tag{1}$$

Equivalently, MSE is defined as replacing σ_{ext} by the scattering coefficient (σ_{scat}) in Equation 1. These quantities can be estimated directly from FIREX-AQ observations using aerosol extinction/scattering coefficients and aerosol mass concentrations from AMS and SP2.

One can discretize the aerosol population by size bins (e.g., those measured by sizing instruments) and using Mie theory assuming spherical and internally mixed particles can estimate σ_{ext} (Bohren & Huffman, 1983) as:

$$\sigma_{\text{ext}} = \frac{\pi}{4} N \sum_i d_i^2 \alpha_i(n_i)\, f_i \tag{2}$$

where N is the total aerosol number concentration, d_i is the diameter of size bin i, $\alpha_i(n_i)$ is the extinction efficiency at diameter d_i with aerosol refractive index n_i, and f_i is the fraction of aerosol number at size bin i, which we refer to here as the aerosol size distribution shape. Similarly, aerosol mass concentration can be computed by discretizing the aerosol size distribution and estimating volume assuming spherical aerosols, and converting to mass using aerosol density per size bin (ρ_i):

$$M = \frac{\pi}{6} N \sum_i d_i^3 \rho_i f_i \tag{3}$$

Substituting Equations 2 and 3 into 1, one obtains:

$$\text{MEE} = \frac{3}{2} \frac{\sum_i d_i^2 \alpha_i(n_i) f_i}{\sum_i d_i^3 \rho_i f_i} \tag{4}$$

This shows that, while MEE can be estimated by two extensive aerosol variables, in theory it is independent of aerosol mass concentrations and is a function of the aerosol size distribution shape, refractive index, and density. Smoke tends to be dominated by accumulation mode aerosol and, in this size range, MEE generally increases with aerosol size and refractive index (Figure S1 in Supporting Information S1). Also, MEE is inversely proportional to aerosol density (Equation 4).

Since MEE, aerosol density, and the size distribution shape were reported from FIREX-AQ observations, the real part of the aerosol refractive index can be estimated numerically using Equation 4 and assuming refractive index and aerosol density don't change across aerosol size for each sample time. This assumption is typically used when estimating refractive index (Hand & Kreidenweis, 2002), and we believe it is reasonable as most of the aerosol mass and volume for FIREX-AQ smoke is in the accumulation mode (Moore et al., 2021) and aerosol modes are usually assumed to be internally mixed. Also, this requires assuming an imaginary part of the refractive index, which is estimated from composition measurements using a volume mixing rule assuming imaginary refractive index for black carbon (BC) equal to 0.71 (Bond & Bergstrom, 2006) and zero for the rest of the species. While this assumption does not include brown carbon (BrC) absorption, the contribution of BrC is expected to be low at mid-visible wavelengths (Zeng et al., 2022). Alternatively, MSE can also be used for this estimation by replacing extinction efficiency with scattering efficiency, which reduces the dependency on aerosol absorption assumptions. Aerosol scattering at 550 nm was used in the calculations, and thus all estimated real(n) values in this study are representative of the mid-visible. Note that the use of aerosol size distribution shape in the computations reduces uncertainties due to loses aerosol sizing instruments have at large concentrations (Liu et al., 2017; Nault et al., 2018).

3. Results

Results are shown for multiple fires and days which are described in Text S2 in Supporting Information S1 along with smoke characteristics that provide context for this analysis. Smoke is separated into three age categories (<2,

2–10, and 10–50 hr old), by OA aerosol concentrations, and by day of emission. Reasons for these choices are outlined in Text S2 in Supporting Information S1.

3.1. MEE Evolution

Figure 1a shows how smoke MEE evolves with age (colors) and organic aerosol concentration (*x*-axis) for smoke emitted on 7 August by the Williams Flats fire. The lowest values of MEE are found for <2-hr old and dense smoke (>500 μg/sm^3) with mean and medians in the range of 2.5–3.2 m^2/g, which increase to 3.5–4 m^2/g for >2-hr old smoke (Figure 1a). Similar trends (but variations in MEE magnitude) are found on other days for fires where comparable OA concentration levels were measured for sustained periods of time (Figures S4a and S4c in Supporting Information S1). On the other hand, the largest values for MEE are found for one-day-old smoke emitted on 7 August (Figure 1a), reaching mean and median values between 6 and 7 m^2/g for OA in the 20–500 μg/m^3 range. Corresponding mean and median MSE values are in the 5.5–6.2 m^2/g range (Figure 1b), which is in the upper end of results from previous field and lab studies (see Section 1). One-day-old smoke MSE is also within literature values. Assuming that smoke sampled had similar emission time, this implies that the MEE of smoke emitted on 7 August changed by a factor of 2–3 over the course of 1 day. This result is relatively insensitive to the corrections to account for OA evaporation and to which aerosol extinction instrument is used to compute MEE (Figures 1a, 1c, and 1d). One-day-old smoke (paired with fresh smoke sampling) was measured in two other instances during FIREX-AQ, but neither of them showed MEE values over 5 m^2/g. (Figures S4b and S4d in Supporting Information S1). Also, MEE enhancements between <2-hr old and 1-day old smoke on these other days were more moderate, with maximum values of a factor ∼2 increase for both days.

As discussed in Section 2.2, MEE is a function of size distribution shape, aerosol density, and refractive index. Assuming log-normal aerosol distributions, the size distribution shape is determined by the mean diameter and the geometric standard deviation. Figures 1a and 1g shows similarities between the evolution of MEE and the volumetric geometric mean diameter (VGMD), both showing a tendency to increase with age and consistent with the literature (see Section 1). While this can explain some of the MEE changes, we note a tendency of VGMD to increase with OA concentration for the more fresh and dense plumes (OA > 500 μg/m^3 for 2–10 hr old, OA > 2,000 μg/m^3 for <2 hr old), while MEE remains roughly constant. The increasing VGMD at higher OA concentrations and the increasing VGMD with smoke age are robust because the same trends are captured by other aerosol size measurements (Figure S5 in Supporting Information S1). On the other hand, OA density decreases with OA concentration for fresh smoke above 500 μg/m^3 (Figure 1h), so it also does not explain the trends in MEE (as aerosol density is inversely proportional to MEE). MEE calculated using observed size distribution shape, a fixed real refractive index of 1.53 for OA, and Mie calculations (Equation 4), can explain only 10% and 37% of the variability (based on R^2) of the observed MEE when using reported and constant OA densities, respectively, and results in a narrower range of mean and median values (5–7 m^2/g, Figures 1e and 1f). Thus, we infer it is highly likely that smoke refractive index is changing to account these unexplained changes in MEE. As seen in Figures 1i–1k, smoke properties such as OA O:C ratio, oxidation state and volatility change significantly with OA concentration and age for smoke emitted on Aug 7th, which further support potential changes in smoke refractive index.

3.2. Real(n) Evolution

Working under the hypothesis that the smoke refractive index can evolve with age, we used the method described in Section 2.2 to estimate the real refractive index for smoke sampled from multiple days and multiple fires. Single-scattering albedo means and medians for smoke from all fires investigated here were in the range of 0.90–0.97 (i.e., absorption accounts for 3%–10% of extinction), implying that MEE is more sensitive to variations of the real (scattering) part of the refractive index (real(n)) and thus it is the parameter that we estimated. This estimation assumes particles are spheres, which is thought to be generally valid for smoke (Martins et al., 1998), and that we assess it produces errors within an acceptable range considering other uncertainties of this study (Text S3 and Figures S6 and S7 in Supporting Information S1). Figure 1l shows the estimated real(n) for the most extreme day of the Williams Flats fire. There is a tendency for decreasing estimated real(n) with increasing OA concentrations above 500 μg/m^3, which results in low (1.37–1.44) values for the highest concentrations of fresh smoke. On the other hand, high values (1.52–1.56) are found for highest concentrations of one-day-old smoke. The latter are closer to the values often found in literature for both smoke and more aged secondary

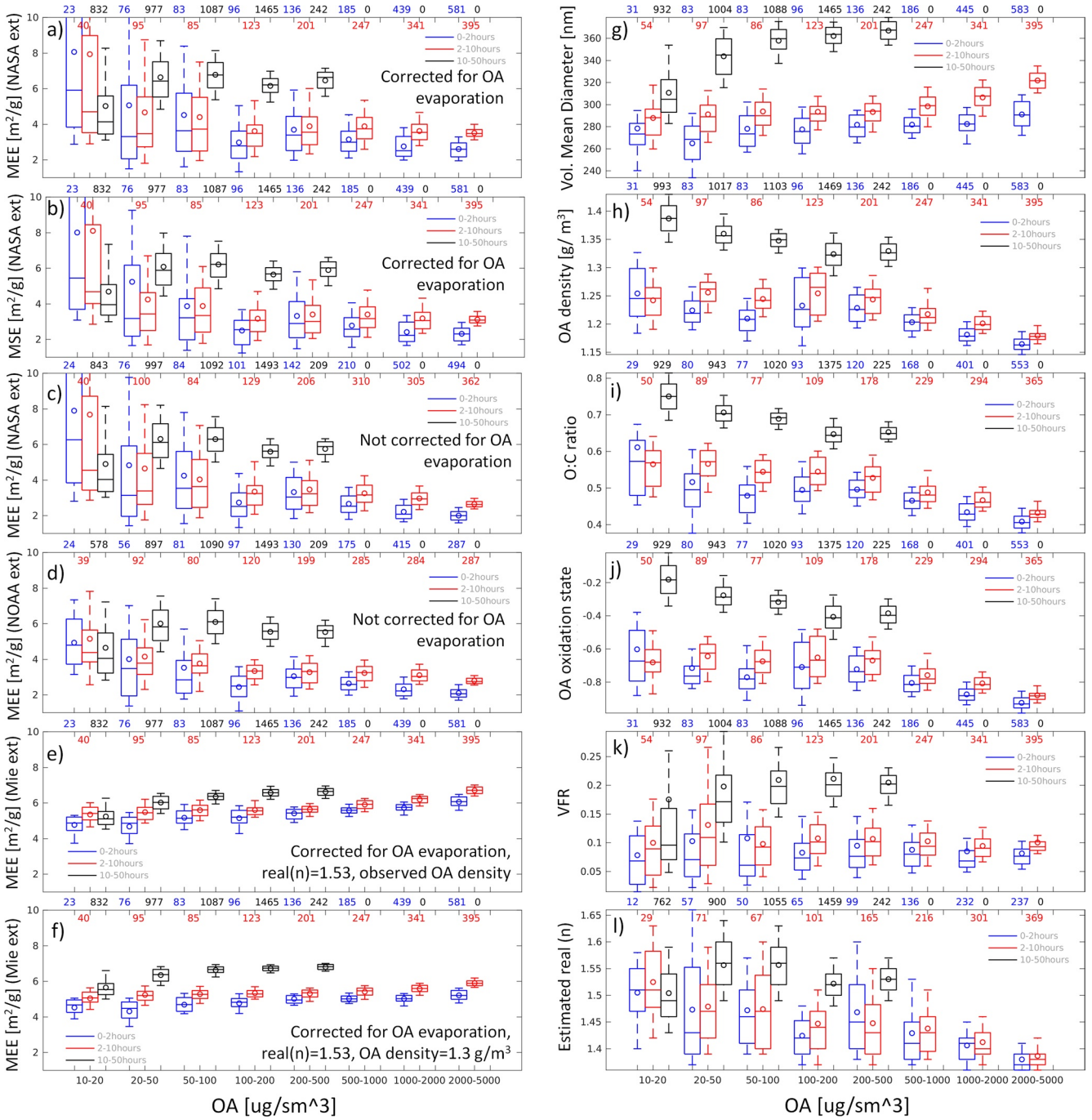

Figure 1. Box and whisker plots showing smoke properties (*y*-axis) as a function of organic aerosol (OA) concentration (*x*-axis) and age (colors) for Williams Flats fire smoke emitted on 7 August. Center solid lines indicate the median, circles represent the mean, boxes indicate upper and lower quartiles, and whiskers show the upper and lower deciles. Number of 1-s data points for each age and OA concentration range is shown on top of each panel using the corresponding box and whisker color. The unit "μg/sm³" stands for μg/m³ at standard temperature and pressure conditions.

organic aerosol (see Section 1). On the other hand, estimated real(n) for fresh smoke at high concentrations is either in the lower end of ranges found in the literature or slightly below. We hypothesize that differences with previous field work can be attributed to previous estimates of real refractive index being not separated by age or OA concentrations, and the tendency of opportunistically sampling plumes that might not correspond to smoke emitted on the same day. Differences with laboratory work could include the sampling at different environmental conditions, especially much lower temperature that can affect the organic aerosol partitioning (see discussion on

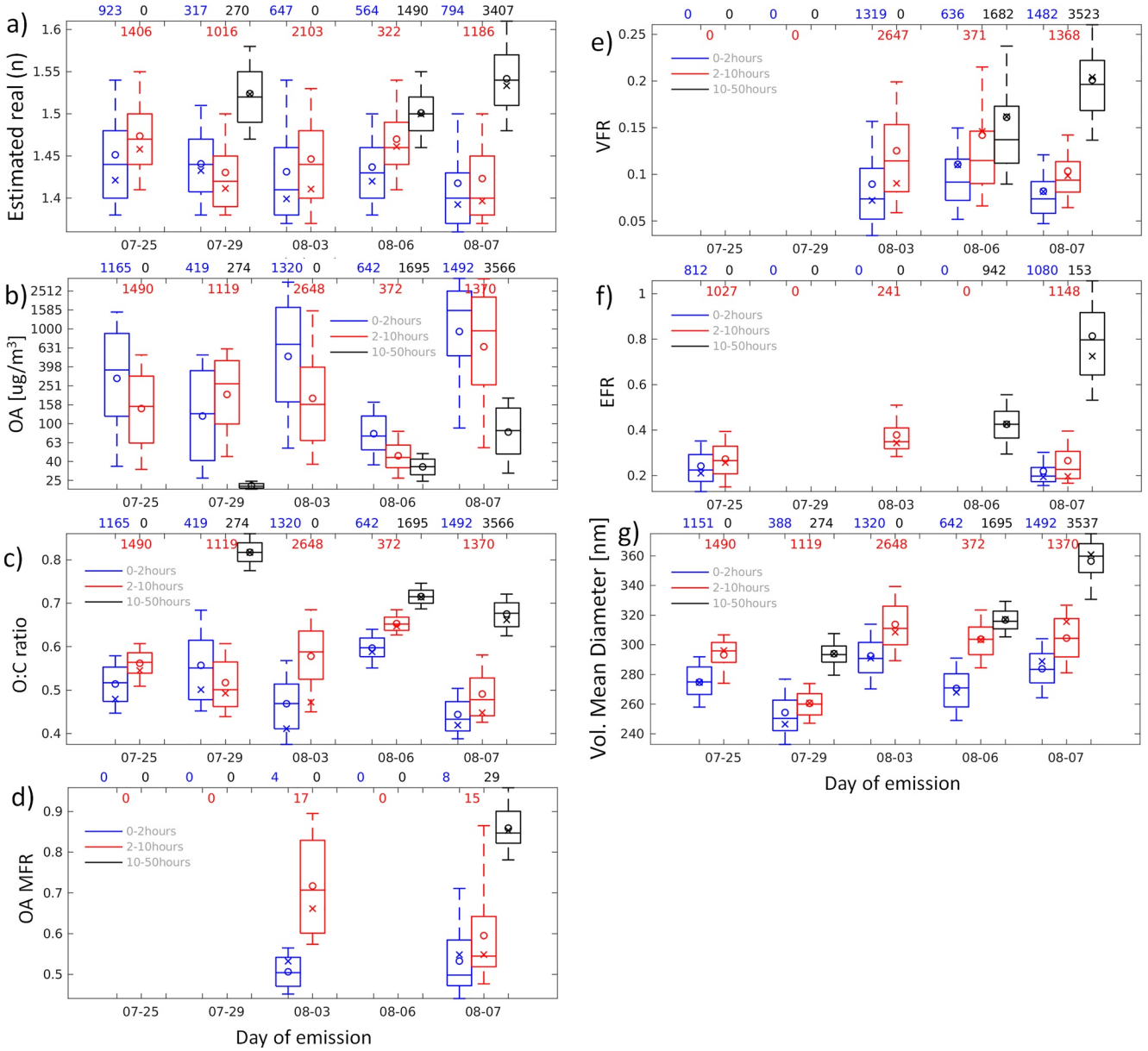

Figure 2. Box and whisker plots as in Figure 1 showing smoke properties as a function of day of emission (*x*-axis) and age (colors) for data from seven flights. The dates correspond to smoke from the following fires: 25 July to Shady, 29 July to Tucker, and 3 August , 6 August, and 7 August to Williams Flats. "*x*"s denote averages weighted by organic aerosol (OA) concentrations. OA concentrations were restricted to above 20 μg/m^3.

following paragraphs). Changing the assumptions on aerosol density and how aerosol size is estimated result in similar real(n) increasing trends with age and decreasing trend with OA above 500 μg/m^3 (Figure S8 in Supporting Information S1), making these trends be the most robust feature of our results. Figure 2 shows the data sorted by emission date to explore the fire-to-fire and day-to-day variations of the estimated real(n) along with potential explanatory variables. This figure shows that the low estimated real(n) for <2 hr smoke tends to be consistent across fires and days, with mean and median values on the 1.40–1.45 range, and slightly lower weighted means as values tend to decrease for large OA concentrations (Figure 1l). Also, estimated real(n) generally increases with age, reaching mean and median values on the range of 1.5–1.54 for one-day-old smoke.

As expected from OA oxidation, there is generally an increasing degree of oxygenation with age for a given day of emission (based on O:C ratio or carbon oxidation state (Kroll et al., 2011), Figures 1i and 1j and 2c). However, the magnitude and rate of increase of the degree of oxygenation can vary substantially for the same age category

among days. These differences are likely explained by differences in smoke concentrations (Figure 2b) as a thicker plume will obscure sunlight and potentially reduce photochemistry. Additionally, under thick smoke the aircraft can access plumes with reduced photochemistry, which in turn can result in sampling of larger gradients (Decker et al., 2021; Xu et al., 2021). For instance, two-to ten-hour-old smoke emitted on 7 August has a lower O:C ratio compared to the other days as it dilutes slower, and <2 hr smoke emitted on 6 August tends to have larger O:C ratio than the other days as concentrations were much lower. The same trend is also found for one-day-old smoke. Additionally, the fire on 7 August exhibited the formation of pyro cumulus creating the possibility for smoke and clouds to interact, which could change OA aging (Ervens et al., 2018). While other differences such as fuel type and flame temperature could also play a role (Cappa et al., 2020), this is less likely as modified combustion efficiency (i.e., a proxy the for relative amounts of flaming and smoldering combustion) from fresh smoke was similar across days (means and medians in the 0.89–0.91 range).

Different measures of smoke volatility are shown in Figures 2d–2f. OA MFR is the more direct measure of volatility, but the sample size was low (due to long integration time and less frequent measurements) and was not available on all days. However, we note that while VFR and EFR show lower corresponding values than OA MFR (which is expected due to the lower operating temperature in the AMS thermodenuder), the trends between different days and age categories are similar and thus can be used to make inferences when OA MFR is missing (see additional verification of this approach on Text S4 in Supporting Information S1). In theory, OA oxidation through addition of functional groups leads to lower volatility, however other processes can either reverse this trend (e.g., fragmentation) or decrease volatility without changes on oxidation (e.g., oligomerization) (N. M. Donahue et al., 2012). Thus, while we do observe a certain degree of correlation between oxidation and the volatility measures (e.g., R^2 between O:C ratio and VFR is 0.77 for means stratifying by age, OA concentration, and day of emissions as in Figures 1 and 2), there are clear differences in some of their trends. For instance, O:C ratio decreases with OA concentration for fresh smoke while volatility tends to be nearly constant (Figures 1i and 1k). Another difference is the very low volatility (high OA, VFR, and EFR) shown for one-day-old smoke emitted on 7 August compared to any other emission day and ages (Figures 2d–2f), while this smoke has a similar or even lower O:C ratio than one-day-old smoke from 6 August (Figure 2c). Figure S9 in Supporting Information S1 shows that indeed day-old smoke emitted on 7 August is less volatile than fresh smoke and not just a reflection of differences in partitioning due to lower OA concentrations. However, we are unable to verify this trend with OA MFR measurements as one-day-old smoke OA MFR was only available for smoke emitted on 7 August.

Various levels of correlation are apparent when comparing the estimated real(n) to O:C ratio, smoke volatility, and aerosol diameter (Figures 1g, 1i, 1j, and 1l, and 2a and 2e–2g). For averages stratified by age, OA concentration, and day of emissions (i.e., circles from Figure 1 but for all days of emission) for the Williams Flats fire, O:C ratio, VFR, and diameter explain 58%, 59%, and 29% of the variability in estimated real(n), respectively (scatterplots and fits in Figure S10 in Supporting Information S1). The multi-linear regression of all these variables explains 63% of the variability. On the other hand, mean O:C ratio, VFR, and diameter by age and emission day (i.e., Figures 2c, 2e, and 2g circles) are able to explain 71%, 96%, and 72% of the variability of mean estimated real(n) (all p-values < 0.05), with the multi-linear regression explaining 96% of the variability. There is a tendency of oxidation to better explain real(n) trends for fresh smoke, while volatility and diameter better explain those for one-day-old smoke. For instance, Figures 1g, 1i, 1j, and 1l shows very similar decreasing trend in O:C ratio and estimated real(n) for fresh smoke as OA concentrations increase, which is not shown by volatility or diameter. On the other hand, the large increase in estimated real(n) for 7 August one-day-old smoke is only captured by the volatility measures and diameter (Figure 2). Estimated real(n) and O:C ratio shown in Figure 2 can be plotted in a scatter plot (Figure S11 in Supporting Information S1) as has been done in studies summarizing literature of OA aging (Figure 8 in Moise et al., 2015), showing that smoke real(n) follows similar trends to that of the oxidation products of azelaic acid (a biogenic molecule used as a proxy for oxidized OA, Cappa et al., 2011) but with a larger range of values. Increasing values of real refractive index with increase in particle size has also been generally found in studies on SOA production from various VOC precursors (Kim et al., 2014; Kim & Paulson, 2013), similar to what is shown here.

These results indicate that there is promise in predicting smoke real(n) based on OA oxidation and volatility, and on particle size. A modeling framework that independently tracks OA volatility and oxidation such as the two-dimensional volatility basis set (2-D-VBS, Chuang & Donahue, 2016; N. M. Donahue et al., 2011; N. M. Donahue et al., 2012) or simplifications of it (Koo et al., 2014) might be suitable for this purpose. However, such a model would have to first accurately predict the oxidation state and volatility of smoke. In this regard, recent

model developments show promise as they are able to track smoke OA oxidation with photochemical aging at high accuracy based on laboratory data (Cappa et al., 2020). Smoke aging in the dark has been found to be an important source of oxidized aerosol (Kodros et al., 2020). This is likely important for wildfire smoke as emissions tend to concentrate in the late afternoon and evening and extreme fire behavior often results in overnight burning (Peterson et al., 2015), thus this needs to be considered when developing models and designing future laboratory studies. As shown earlier, proper representation of aerosol size is also important for resolving MEE. Thus, given the correlation of diameter and refractive index, evaluating and developing models to resolve particle diameter (e.g., June et al., 2022) can also support parameterizations of real refractive index evolution.

Perhaps the most challenging feature for future models to represent would be the strong decrease in volatility for 7 August emitted smoke that is not explained by oxidation changes. While we are currently not able to fully explain this behavior, we can provide potential hypotheses for future work to explore. Observed smoke emitted on Aug 7th was characterized by having the highest OA concentrations and being emitted (and sampled) at higher altitudes (Figure S2 in Supporting Information S1) and thus lower temperature (T) than smoke emitted on other days (mean Ts for 3, 6, and 7 August are 281, 285, and 270 K, respectively). Due to the semi-volatile nature of the smoke, these conditions would lead to a large fraction of the higher volatility organics to be in the particle phase even after 2 hours of since emission, while they are mostly in the gas phase for emissions on the other days (Figure S12 in Supporting Information S1). Thus, differences between products of gas phase oxidation and condensed phase reactions (e.g., heterogeneous uptake of oxidants, reactions among organics, and acid base reactions) could be playing a role in the resulting volatility. Oligomerization is a process where small reactive organic molecules (monomers) can create higher carbon number association products (oligomers) with significantly lower volatility and negligible changes to oxidation state, and it's thought to occur mostly in the condensed phase (De Haan et al., 2009; Kalberer et al., 2004; Tolocka et al., 2004). Additionally, the fire on 7 August exhibited the formation of pyro cumulus. Previous studies have found that aqueous chemistry can promote oligomerization reactions in ways that are not accessible to gas-phase processing only (Altieri et al., 2008; Boone et al., 2015), providing additional pathways for oligomerization to occur. Thus, conditions on 7 August could be favoring the occurrence of oligomerization resulting in the large decreases in smoke volatility.

4. Conclusions and Future Directions

MEE is an important aerosol optical property to understand in the context of smoke evolution. The FIREX-AQ field campaign sampled isolated wildfire smoke from multiple fires with ages ranging from below 1 hr up to over one-day-old which allows a detailed study of MEE progression. We find that for the day of more extreme fire development of the Williams Flats fire, MEE shows the largest changes, with mean MEE in the range of 2.5–3.2 m^2/g for thick smoke younger than 2 hr, up to values of 6–7 m^2/g for 1-day-old smoke. Fresh smoke MEE shows similar behavior for other days and other fires, but such high MEE values for one-day-old smoke are not reproduced any other day and are in the upper end of values found in the literature. Increases in aerosol size with age partially explain these trends but are insufficient to fully explain the observed variability and range of MEE. Thus, we conclude that changes in the smoke refractive index are needed to explain the trends in MEE. Using observations and Mie theory, we derive expected values of the real part of the smoke refractive index (real(n)) to match the observed MEE. We find that estimated real(n) depends strongly on aerosol mass concentration, age, and day of emission. Mean extreme values of 1.37–1.44 for high OA concentrations (>500 $\mu g/m^3$) of <2 hr old smoke, and 1.52–1.56 for one-day-old smoke >50 $\mu g/m^3$ are found, with the former being in the lower range or below previous studies and the latter closer to averages found in the literature. Considering all fires and OA concentrations >20 $\mu g/m^3$, average estimated real(n) increases from 1.40–1.45 to 1.5–1.54 from <2 hr of age to 1-day-old smoke. Additionally, derived real(n) is correlated with increases of OA oxidation and aerosol size, and decreases of smoke volatility, to a point where the mean behavior of real(n) by emission day and age category can be well explained by these variables. While there are multiple uncertainties inherent to this analysis (e.g., instrument uncertainty, inlet evaporation, assumption of aerosol density, Mie theory assumptions applied to smoke aerosol), the trends found appear robust and warrant further investigation.

These results have multiple implications. Extreme fire behavior is more often being observed in recent fire seasons. For instance, the day the Williams Flats showed the more extreme behavior (7 August) it burned ~5,200 Ha, while large non-complex fires in 2020 such as Creek, Cameron Peak, Dolan, East Troublesome, and Holiday Farm burned similar or larger areas on multiple days. Additionally, fires are expected to inject more smoke at

greater heights as wildfire activity intensify (Wilmot et al., 2022). Thus, the conditions generating large differences in MEE and real(n) between fresh and aged smoke found here for smoke emitted on 7 August are expected to happen more often. However, given the limited sample of large fires studied here, this needs to be confirmed by future research. A review of smoke forecasting systems showed that only a minority of them track aerosol size, and little to none track changes of OA refractive index with age (Ye et al., 2021). Thus, this increases uncertainties when constraining smoke aerosol mass using satellite AOD retrievals as proper parameterization of aerosol optical properties is required. Future studies need to evaluate the capability and performance of atmospheric composition models to reproduce smoke size changes with age, but also parameterization development is needed to fully characterize the changes of refractive index with age. Low-cost sensors measuring surface $PM_{2.5}$ generally convert aerosol scattering into $PM_{2.5}$ mass concentrations, and thus an assessment of their calibration and conversion accuracy under different smoke concentrations and ages is needed. Additionally, we expect this work to motivate laboratory studies that would try to replicate the conditions generating low real(n), and the low volatility associated to high real(n), to understand the chemical process behind them and support model development.

Conflict of Interest

The authors declare no conflicts of interest relevant to this study.

Data Availability Statement

Flight observational data from FIREX-AQ, along with the DIAL-HSRL data during the field campaign are archived by NASA/LARC/SD/ASDC (https://doi.org/10.5067/SUBORBITAL/FIREXAQ2019/DATA001, https://www-air.larc.nasa.gov/missions/firex-aq/). The database for database of tri-axial ellipsoid optical properties was provided by Prof. Ping Yang (Texas A&M University).

Acknowledgments
We acknowledge Charles Brock for provided insightful comments in the preparation of the manuscript. This work has been supported by the following grants: NASA 80NSSC18K0629, NASA 80NSSC18K0630 NASA 80NSSC20K1650, NASA 80NSSC19K0124, NOAA NA18OAR4310107, NSF 2013461.

References

Aldhaif, A. M., Stahl, C., Braun, R. A., Moghaddam, M. A., Shingler, T., Crosbie, E., et al. (2018). Characterization of the real part of dry aerosol refractive index over North America from the surface to 12 km. *Journal of Geophysical Research: Atmospheres*, *123*(15), 8283–8300. https://doi.org/10.1029/2018jd028504

Altieri, K. E., Seitzinger, S. P., Carlton, A. G., Turpin, B. J., Klein, G. C., & Marshall, A. G. (2008). Oligomers formed through in-cloud methylglyoxal reactions: Chemical composition, properties, and mechanisms investigated by ultra-high resolution FT-ICR mass spectrometry. *Atmospheric Environment*, *42*(7), 1476–1490. https://doi.org/10.1016/j.atmosenv.2007.11.015

Bian, Q., Ford, B., Pierce, J. R., & Kreidenweis, S. M. (2020). A decadal climatology of chemical, physical, and optical properties of ambient smoke in the Western and southeastern United States. *Journal of Geophysical Research: Atmospheres*, *125*(1), e2019JD031372. https://doi.org/10.1029/2019JD031372

Bohren, C. F., & Huffman, D. R. (1983). *Absorption and scattering of light by small particles*. Wiley.

Bond, T. C., & Bergstrom, R. W. (2006). Light absorption by carbonaceous particles: An investigative review. *Aerosol Science and Technology*, *40*(1), 27–67. https://doi.org/10.1080/02786820500421521

Boone, E. J., Laskin, A., Laskin, J., Wirth, C., Shepson, P. B., Stirm, B. H., & Pratt, K. A. (2015). Aqueous processing of atmospheric organic particles in cloud water collected via aircraft sampling. *Environmental Science and Technology*, *49*(14), 8523–8530. https://doi.org/10.1021/acs.est.5b01639

Canagaratna, M. R., Jimenez, J. L., Kroll, J. H., Chen, Q., Kessler, S. H., Massoli, P., et al. (2015). Elemental ratio measurements of organic compounds using aerosol mass spectrometry: Characterization, improved calibration, and implications. *Atmospheric Chemistry and Physics*, *15*(1), 253–272. https://doi.org/10.5194/acp-15-253-2015

Cappa, C. D., Che, D. L., Kessler, S. H., Kroll, J. H., & Wilson, K. R. (2011). Variations in organic aerosol optical and hygroscopic properties upon heterogeneous OH oxidation. *Journal of Geophysical Research*, *116*(D15), D15204. https://doi.org/10.1029/2011JD015918

Cappa, C. D., Lim, C. Y., Hagan, D. H., Coggon, M., Koss, A., Sekimoto, K., et al. (2020). Biomass-burning-derived particles from a wide variety of fuels – Part 2: Effects of photochemical aging on particle optical and chemical properties. *Atmospheric Chemistry and Physics*, *20*(14), 8511–8532. https://doi.org/10.5194/acp-20-8511-2020

Cheeseman, M., Ford, B., Volckens, J., Lyapustin, A., & Pierce, J. R. (2020). The relationship between MAIAC smoke plume heights and surface PM. *Geophysical Research Letters*, *47*(17), e2020GL088949. https://doi.org/10.1029/2020GL088949

Chuang, W. K., & Donahue, N. M. (2016). A two-dimensional volatility basis set – Part 3: Prognostic modeling and NOx dependence. *Atmospheric Chemistry and Physics*, *16*(1), 123–134. https://doi.org/10.5194/acp-16-123-2016

Deb, P., Moradkhani, H., Abbaszadeh, P., Kiem, A. S., Engström, J., Keellings, D., & Sharma, A. (2020). Causes of the widespread 2019–2020 Australian bushfire season. *Earth's Future*, *8*(11), e2020EF001671. https://doi.org/10.1029/2020EF001671

Decker, Z. C. J., Robinson, M. A., Barsanti, K. C., Bourgeois, I., Coggon, M. M., DiGangi, J. P., et al. (2021). Nighttime and daytime dark oxidation chemistry in wildfire plumes: An observation and model analysis of FIREX-AQ aircraft data. *Atmospheric Chemistry and Physics*, *21*, 16293–16317. https://doi.org/10.5194/acp-21-16293-2021

De Haan, D. O., Tolbert, M. A., & Jimenez, J. L. (2009). Atmospheric condensed-phase reactions of glyoxal with methylamine. *Geophysical Research Letters*, *36*(11), L11819. https://doi.org/10.1029/2009GL037441

Delp, W. W., & Singer, B. C. (2020). Wildfire smoke adjustment factors for low-cost and professional PM2.5 monitors with optical sensors. *Sensors*, *20*(13), 3683. https://doi.org/10.3390/s20133683

Donahue, N. M., Epstein, S. A., Pandis, S. N., & Robinson, A. L. (2011). A two-dimensional volatility basis set: 1. Organic-aerosol mixing thermodynamics. *Atmospheric Chemistry and Physics*, *11*(7), 3303–3318. https://doi.org/10.5194/acp-11-3303-2011

Donahue, N. M., Kroll, J. H., Pandis, S. N., & Robinson, A. L. (2012). A two-dimensional volatility basis set – Part 2: Diagnostics of organic-aerosol evolution. *Atmospheric Chemistry and Physics*, *12*(2), 615–634. https://doi.org/10.5194/acp-12-615-2012

Ervens, B., Sorooshian, A., Aldhaif, A. M., Shingler, T., Crosbie, E., Ziemba, L., et al. (2018). Is there an aerosol signature of chemical cloud processing? *Atmospheric Chemistry and Physics*, *18*(21), 16099–16119. https://doi.org/10.5194/acp-18-16099-2018

Espinosa, W. R., Remer, L. A., Dubovik, O., Ziemba, L., Beyersdorf, A., Orozco, D., et al. (2017). Retrievals of aerosol optical and microphysical properties from Imaging Polar Nephelometer scattering measurements. *Atmospheric Measurement Techniques*, *10*(3), 811–824. https://doi.org/10.5194/amt-10-811-2017

Forehead, H., Barthelemy, J., Arshad, B., Verstaevel, N., Price, O., & Perez, P. (2020). Traffic exhaust to wildfires: PM2.5 measurements with fixed and portable, low-cost LoRaWAN-connected sensors. *PLoS One*, *15*(4), e0231778. https://doi.org/10.1371/journal.pone.0231778

Guo, H., Campuzano-Jost, P., Nault, B. A., Day, D. A., Schroder, J. C., Kim, D., et al. (2021). The importance of size ranges in aerosol instrument intercomparisons: A case study for the atmospheric tomography mission. *Atmospheric Measurement Techniques*, *14*(5), 3631–3655. https://doi.org/10.5194/amt-14-3631-2021

Hand, J. L., & Kreidenweis, S. M. (2002). A new method for retrieving particle refractive index and effective density from aerosol size distribution data. *Aerosol Science and Technology*, *36*(10), 1012–1026. https://doi.org/10.1080/02786820290092276

Higuera, P. E., & Abatzoglou, J. T. (2021). Record-setting climate enabled the extraordinary 2020 fire season in the Western United States. *Global Change Biology*, *27*, 1–2. https://doi.org/10.1111/gcb.15388

Hodshire, A. L., Ramnarine, E., Akherati, A., Alvarado, M. L., Farmer, D. K., Jathar, S. H., et al. (2021). Dilution impacts on smoke aging: Evidence in biomass burning observation project (BBOP) data. *Atmospheric Chemistry and Physics*, *21*(9), 6839–6855. https://doi.org/10.5194/acp-21-6839-2021

Ichoku, C., & Ellison, L. (2014). Global top-down smoke-aerosol emissions estimation using satellite fire radiative power measurements. *Atmospheric Chemistry and Physics*, *14*(13), 6643–6667. https://doi.org/10.5194/acp-14-6643-2014

Jin, Y., Goulden, M. L., Faivre, N., Veraverbeke, S., Sun, F., Hall, A., et al. (2015). Identification of two distinct fire regimes in southern California: Implications for economic impact and future change. *Environmental Research Letters*, *10*(9), 094005. https://doi.org/10.1088/1748-9326/10/9/094005

June, N. A., Hodshire, A. L., Wiggins, E. B., Winstead, E. L., Robinson, C. E., Thornhill, K. L., et al. (2022). Aerosol size distribution changes in FIREX-AQ biomass burning plumes: The impact of plume concentration on coagulation and OA condensation/evaporation. *Atmospheric Chemistry and Physics Discussions*, 1–35. https://doi.org/10.5194/acp-2022-349

Kalberer, M., Paulsen, D., Sax, M., Steinbacher, M., Dommen, J., Prevot, A. S. H., et al. (2004). Identification of polymers as major components of atmospheric organic aerosols. *Science*, *303*(5664), 1659–1662. https://doi.org/10.1126/science.1092185

Kim, H., Liu, S., Russell, L. M., & Paulson, S. E. (2014). Dependence of real refractive indices on O:C, H:C and mass fragments of secondary organic aerosol generated from ozonolysis and photooxidation of limonene and α-pinene. *Aerosol Science and Technology*, *48*(5), 498–507. https://doi.org/10.1080/02786826.2014.893278

Kim, H., & Paulson, S. E. (2013). Real refractive indices and volatility of secondary organic aerosol generated from photooxidation and ozonolysis of limonene, α-pinene and toluene. *Atmospheric Chemistry and Physics*, *13*(15), 7711–7723. https://doi.org/10.5194/acp-13-7711-2013

Kleinman, L. I., Sedlacek, A. J., Iii, Adachi, K., Buseck, P. R., Collier, S., Dubey, M. K., et al. (2020). Rapid evolution of aerosol particles and their optical properties downwind of wildfires in the Western US. *Atmospheric Chemistry and Physics*, *20*(21), 13319–13341. https://doi.org/10.5194/acp-20-13319-2020

Kodros, J. K., Papanastasiou, D. K., Paglione, M., Masiol, M., Squizzato, S., Florou, K., et al. (2020). Rapid dark aging of biomass burning as an overlooked source of oxidized organic aerosol. *Proceedings of the National Academy of Sciences*, *117*(52), 33028–33033. https://doi.org/10.1073/pnas.2010365117

Koo, B., Knipping, E., & Yarwood, G. (2014). 1.5-Dimensional volatility basis set approach for modeling organic aerosol in CAMx and CMAQ. *Atmospheric Environment*, *95*, 158–164. https://doi.org/10.1016/j.atmosenv.2014.06.031

Kroll, J. H., Donahue, N. M., Jimenez, J. L., Kessler, S. H., Canagaratna, M. R., Wilson, K. R., et al. (2011). Carbon oxidation state as a metric for describing the chemistry of atmospheric organic aerosol. *Nature Chemistry*, *3*(2), 133–139. https://doi.org/10.1038/nchem.948

Kuwata, M., Zorn, S. R., & Martin, S. T. (2012). Using elemental ratios to predict the density of organic material composed of carbon, hydrogen, and oxygen. *Environmental Science and Technology*, *46*(2), 787–794. https://doi.org/10.1021/es202525q

Laing, J. R., Jaffe, D. A., & Hee, J. R. (2016). Physical and optical properties of aged biomass burning aerosol from wildfires in Siberia and the Western USA at the Mt. Bachelor Observatory. *Atmospheric Chemistry and Physics*, *16*(23), 15185–15197. https://doi.org/10.5194/acp-16-15185-2016

Lamb, K. D., Perring, A. E., Samset, B., Peterson, D., Davis, S., Anderson, B. E., et al. (2018). Estimating source region influences on black carbon abundance, microphysics, and radiative effect observed over South Korea. *Journal of Geophysical Research: Atmospheres*, *123*(13), 527–513. https://doi.org/10.1029/2018jd029257

Langridge, J. M., Richardson, M. S., Lack, D., Law, D., & Murphy, D. M. (2011). Aircraft instrument for comprehensive characterization of aerosol optical properties, Part I: Wavelength-dependent optical extinction and its relative humidity dependence measured using cavity ringdown spectroscopy. *Aerosol Science and Technology*, *45*(11), 1305–1318. https://doi.org/10.1080/02786826.2011.592745

Levin, E. J. T., McMeeking, G. R., Carrico, C. M., Mack, L. E., Kreidenweis, S. M., Wold, C. E., et al. (2010). Biomass burning smoke aerosol properties measured during Fire Laboratory at Missoula Experiments (FLAME). *Journal of Geophysical Research*, *115*(D18), D18210. https://doi.org/10.1029/2009JD013601

Liu, X., Huey, L. G., Yokelson, R. J., Selimovic, V., Simpson, I. J., Müller, M., et al. (2017). Airborne measurements of Western U.S. wildfire emissions: Comparison with prescribed burning and air quality implications. *Journal of Geophysical Research: Atmospheres*, *122*(11), 6108–6129. https://doi.org/10.1002/2016JD026315

Martins, J. V., Artaxo, P., Hobbs, P., Liousse, C., Cachier, H., Kaufman, Y., & Plana-Fattori, A. (1996). Particle size distributions, elemental compositions, carbon measurements, and optical properties of smoke from biomass burning in the Pacific Northwest of the Unites States. In *Biomass burning and global change*. MIT Press.

Martins, J. V., Hobbs, P. V., Weiss, R. E., & Artaxo, P. (1998). Sphericity and morphology of smoke particles from biomass burning in Brazil. *Journal of Geophysical Research*, *103*(D24), 32051–32057. https://doi.org/10.1029/98JD01153

Mirzaei, M., Bertazzon, S., Couloigner, I., Farjad, B., & Ngom, R. (2020). Estimation of local daily PM2.5 concentration during wildfire episodes: Integrating MODIS AOD with multivariate linear mixed effect (LME) models. *Air Quality, Atmosphere & Health*, *13*(2), 173–185. https://doi.org/10.1007/s11869-019-00780-y

Moise, T., Flores, J. M., & Rudich, Y. (2015). Optical properties of secondary organic aerosols and their changes by chemical processes. *Chemical Reviews*, *115*(10), 4400–4439. https://doi.org/10.1021/cr5005259

Moore, R. H., Wiggins, E. B., Ahern, A. T., Zimmerman, S., Montgomery, L., Campuzano Jost, P., et al. (2021). Sizing response of the Ultra-High Sensitivity Aerosol Size Spectrometer (UHSAS) and Laser Aerosol Spectrometer (LAS) to changes in submicron aerosol composition and refractive index. *Atmospheric Measurement Techniques Discussion*, 1–36. https://doi.org/10.5194/amt-2021-21

Moosmüller, H., Chakrabarty, R. K., & Arnott, W. P. (2009). Aerosol light absorption and its measurement: A review. *Journal of Quantitative Spectroscopy and Radiative Transfer*, *110*(11), 844–878. https://doi.org/10.1016/j.jqsrt.2009.02.035

Nault, B. A., Campuzano-Jost, P., Day, D. A., Schroder, J. C., Anderson, B., Beyersdorf, A. J., et al. (2018). Secondary organic aerosol production from local emissions dominates the organic aerosol budget over Seoul, South Korea, during KORUS-AQ. *Atmospheric Chemistry and Physics*, *18*(24), 17769–17800. https://doi.org/10.5194/acp-18-17769-2018

O'Dell, K., Bilsback, K., Ford, B., Martenies, S. E., Magzamen, S., Fischer, E. V., & Pierce, J. R. (2021). Estimated mortality and morbidity attributable to smoke plumes in the United States: Not just a Western US problem. *GeoHealth*, *5*(9), e2021GH000457. https://doi.org/10.1029/2021GH000457

Peterson, D. A., Fromm, M. D., McRae, R. H. D., Campbell, J. R., Hyer, E. J., Taha, G., et al. (2021). Australia's Black Summer pyrocumulonimbus super outbreak reveals potential for increasingly extreme stratospheric smoke events. *npj Climate and Atmospheric Science*, *4*(1), 38. https://doi.org/10.1038/s41612-021-00192-9

Peterson, D. A., Hyer, E. J., Campbell, J. R., Fromm, M. D., Hair, J. W., Butler, C. F., & Fenn, M. A. (2015). The 2013 rim fire: Implications for predicting extreme fire spread, pyroconvection, and smoke emissions. *Bulletin of the American Meteorological Society*, *96*(2), 229–247. https://doi.org/10.1175/bams-d-14-00060.1

Randerson, J. T., Liu, H., Flanner, M. G., Chambers, S. D., Jin, Y., Hess, P. G., et al. (2006). The impact of boreal forest fire on climate warming. *Science*, *314*(5802), 1130–1132. https://doi.org/10.1126/science.1132075

Reid, C. E., Brauer, M., Johnston, F. H., Jerrett, M., Balmes, J. R., & Elliott, C. T. (2016). Critical review of health impacts of wildfire smoke exposure. *Environmental Health Perspectives*, *124*(9), 1334–1343. https://doi.org/10.1289/ehp.1409277

Reid, J. S., Eck, T. F., Christopher, S. A., Koppmann, R., Dubovik, O., Eleuterio, D. P., et al. (2005). A review of biomass burning emissions part III: Intensive optical properties of biomass burning particles. *Atmospheric Chemistry and Physics*, *5*(3), 827–849. https://doi.org/10.5194/acp-5-827-2005

Reid, J. S., Hobbs, P. V., Ferek, R. J., Blake, D. R., Martins, J. V., Dunlap, M. R., & Liousse, C. (1998). Physical, chemical, and optical properties of regional hazes dominated by smoke in Brazil. *Journal of Geophysical Research*, *103*(D24), 32059–32080. https://doi.org/10.1029/98JD00458

Reid, J. S., Koppmann, R., Eck, T. F., & Eleuterio, D. P. (2005). A review of biomass burning emissions part II: Intensive physical properties of biomass burning particles. *Atmospheric Chemistry and Physics*, *5*(3), 799–825. https://doi.org/10.5194/acp-5-799-2005

Saide, P. E., Peterson, D., da Silva, A., Anderson, B., Ziemba, L. D., Diskin, G., et al. (2015). Revealing important nocturnal and day-to-day variations in fire smoke emissions through a multiplatform inversion. *Geophysical Research Letters*, *42*(9), 3609–3618. 2015GL063737. https://doi.org/10.1002/2015gl063737

Spracklen, D. V., Logan, J. A., Mickley, L. J., Park, R. J., Yevich, R., Westerling, A. L., & Jaffe, D. A. (2007). Wildfires drive interannual variability of organic carbon aerosol in the Western U.S. in summer. *Geophysical Research Letters*, *34*(16). https://doi.org/10.1029/2007GL030037

Spracklen, D. V., Mickley, L. J., Logan, J. A., Hudman, R. C., Yevich, R., Flannigan, M. D., & Westerling, A. L. (2009). Impacts of climate change from 2000 to 2050 on wildfire activity and carbonaceous aerosol concentrations in the Western. *United States*, *114*(D20), D20301. https://doi.org/10.1029/2008jd010966

Sumlin, B. J., Heinson, Y. W., Shetty, N., Pandey, A., Pattison, R. S., Baker, S., et al. (2018). UV–Vis–IR spectral complex refractive indices and optical properties of brown carbon aerosol from biomass burning. *Journal of Quantitative Spectroscopy and Radiative Transfer*, *206*, 392–398. https://doi.org/10.1016/j.jqsrt.2017.12.009

Tolocka, M. P., Jang, M., Ginter, J. M., Cox, F. J., Kamens, R. M., & Johnston, M. V. (2004). Formation of oligomers in secondary organic aerosol. *Environmental Science and Technology*, *38*(5), 1428–1434. https://doi.org/10.1021/es035030r

Wilmot, T. Y., Mallia, D. V., Hallar, A. G., & Lin, J. C. (2022). Wildfire plumes in the Western US are reaching greater heights and injecting more aerosols aloft as wildfire activity intensifies. *Scientific Reports*, *12*(1), 12400. https://doi.org/10.1038/s41598-022-16607-3

Womack, C. C., Manfred, K. M., Wagner, N. L., Adler, G., Franchin, A., Lamb, K. D., et al. (2021). Complex refractive indices in the ultraviolet and visible spectral region for highly absorbing non-spherical biomass burning aerosol. *Atmospheric Chemistry and Physics*, *21*(9), 7235–7252. https://doi.org/10.5194/acp-21-7235-2021

Xu, L., Crounse, J. D., Vasquez, K. T., Allen, H., Wennberg, P. O., Bourgeois, I., et al. (2021). Ozone chemistry in Western U.S. wildfire plumes. *Science Advances*, *7*(50), eabl3648. https://doi.org/10.1126/sciadv.abl3648

Ye, X., Arab, P., Ahmadov, R., James, E., Grell, G. A., Pierce, B., et al. (2021). Evaluation and intercomparison of wildfire smoke forecasts from multiple modeling systems for the 2019 Williams Flats fire. *Atmospheric Chemistry and Physics*, *21*(18), 14427–14469. https://doi.org/10.5194/acp-21-14427-2021

Zeng, L., Dibb, J., Scheuer, E., Katich, J. M., Schwarz, J. P., Bourgeois, I., et al. (2022). Characteristics and evolution of Brown carbon in Western United States Wildfires. *Atmospheric Chemistry and Physics Discussions*, 1–45. https://doi.org/10.5194/acp-2022-70

Ziemba, L. D., Lee Thornhill, K., Ferrare, R., Barrick, J., Beyersdorf, A. J., Chen, G., et al. (2013). Airborne observations of aerosol extinction by in situ and remote-sensing techniques: Evaluation of particle hygroscopicity. *Geophysical Research Letters*, *40*(2), 417–422. https://doi.org/10.1029/2012gl054428

References From the Supporting Information

Adachi, K., Dibb, J. E., Scheuer, E., Katich, J. M., Schwarz, J. P., Perring, A. E., et al. (2022). Fine ash-bearing particles as a major aerosol component in biomass burning smoke. *Journal of Geophysical Research: Atmospheres*, *127*(2), e2021JD035657. https://doi.org/10.1029/2021JD035657

Bahreini, R., Ervens, B., Middlebrook, A. M., Warneke, C., de Gouw, J. A., DeCarlo, P. F., et al. (2009). Organic aerosol formation in urban and industrial plumes near Houston and Dallas, Texas. *Journal of Geophysical Research*, *114*, D00F16. https://doi.org/10.1029/2008JD011493

Bourgeois, I., Peischl, J., Neuman, J. A., Brown, S. S., Allen, H. M., Campuzano-Jost, P., et al. (2022). Comparison of airborne measurements of NO, NO2, HONO, NOy and CO during FIREX-AQ. *Atmospheric Measurement Techniques Discussions*, 1–47. https://doi.org/10.5194/amt-2021-432

Burton, S. P., Ferrare, R. A., Hostetler, C. A., Hair, J. W., Rogers, R. R., Obland, M. D., et al. (2012). Aerosol classification using airborne High Spectral Resolution Lidar measurements – Methodology and examples. *Atmospheric Measurement Techniques*, *5*(1), 73–98. https://doi.org/10.5194/amt-5-73-2012

Burton, S. P., Hair, J. W., Kahnert, M., Ferrare, R. A., Hostetler, C. A., Cook, A. L., et al. (2015). Observations of the spectral dependence of linear particle depolarization ratio of aerosols using NASA Langley airborne High Spectral Resolution Lidar. *Atmospheric Chemistry and Physics*, *15*(23), 13453–13473. https://doi.org/10.5194/acp-15-13453-2015

Cappa, C. D. (2010). A model of aerosol evaporation kinetics in a thermodenuder. *Atmospheric Measurement Techniques*, *3*, 579–592. https://doi.org/10.5194/amt-3-579-2010

Cattrall, C., Reagan, J., Thome, K., & Dubovik, O. (2005). Variability of aerosol and spectral lidar and backscatter and extinction ratios of key aerosol types derived from selected Aerosol Robotic Network locations. *Journal of Geophysical Research*, *110*(D10), D10S11. https://doi.org/10.1029/2004JD005124

DeCarlo, P. F., Dunlea, E. J., Kimmel, J. R., Aiken, A. C., Sueper, D., Crounse, J., et al. (2008). Fast airborne aerosol size and chemistry measurements above Mexico City and Central Mexico during the MILAGRO campaign. *Atmospheric Chemistry and Physics*, *8*(14), 4027–4048. https://doi.org/10.5194/acp-8-4027-2008

Donahue, N. M., Robinson, A. L., & Pandis, S. N. (2009). Atmospheric organic particulate matter: From smoke to secondary organic aerosol. *Atmospheric Environment*, *43*(1), 94–106. https://doi.org/10.1016/j.atmosenv.2008.09.055

Hair, J., Hostetler, C., Cook, A., Harper, D., Notari, A., Fenn, M., et al. (2018). New capability for ozone dial profiling measurements in the troposphere and lower stratosphere from aircraft. *EPJ Web of Conferences*, *176*, 01006. https://doi.org/10.1051/epjconf/201817601006

Heim, E. W., Dibb, J., Scheuer, E., Jost, P. C., Nault, B. A., Jimenez, J. L., et al. (2020). Asian dust observed during KORUS-AQ facilitates the uptake and incorporation of soluble pollutants during transport to South Korea. *Atmospheric Environment*, *224*, 117305. https://doi.org/10.1016/j.atmosenv.2020.117305

Holmes, C. D., Fite, C. H., Agastra, A., Schwarz, J., Yokelson, R., Bui, T. P., & Peterson, D. (2021). Critical evaluation of smoke age inferred from different methods during FIREX-AQ. in preparation.

Huang, Y., Kok, J. F., Kandler, K., Lindqvist, H., Nousiainen, T., Sakai, T., et al. (2020). Climate models and remote sensing retrievals neglect substantial desert dust asphericity. *Geophysical Research Letters*, *47*(6), e2019GL086592. https://doi.org/10.1029/2019GL086592

Kupc, A., Williamson, C., Wagner, N. L., Richardson, M., & Brock, C. A. (2018). Modification, calibration, and performance of the Ultra-High Sensitivity Aerosol Spectrometer for particle size distribution and volatility measurements during the Atmospheric Tomography Mission (ATom) airborne campaign. *Atmospheric Measurement Techniques*, *11*(1), 369–383. https://doi.org/10.5194/amt-11-369-2018

Lambe, A. T., Ahern, A. T., Williams, L. R., Slowik, J. G., Wong, J. P. S., Abbatt, J. P. D., et al. (2011). Characterization of aerosol photooxidation flow reactors: Heterogeneous oxidation, secondary organic aerosol formation and cloud condensation nuclei activity measurements. *Atmospheric Measurement Techniques*, *4*(3), 445–461. https://doi.org/10.5194/amt-4-445-2011

Liu, L., & Mishchenko, M. I. (2020). Spectrally dependent linear depolarization and lidar ratios for nonspherical smoke aerosols. *Journal of Quantitative Spectroscopy and Radiative Transfer*, *248*, 106953. https://doi.org/10.1016/j.jqsrt.2020.106953

May, A. A., Levin, E. J. T., Hennigan, C. J., Riipinen, I., Lee, T., Collett, J. L., Jr., et al. (2013). Gas-particle partitioning of primary organic aerosol emissions: 3. Biomass burning. *Journal of Geophysical Research: Atmospheres*, *118*, 11327–11338. https://doi.org/10.1002/jgrd.50828

Meng, Z., Yang, P., Kattawar, G. W., Bi, L., Liou, K. N., & Laszlo, I. (2010). Single-scattering properties of tri-axial ellipsoidal mineral dust aerosols: A database for application to radiative transfer calculations. *Journal of Aerosol Science*, *41*(5), 501–512. https://doi.org/10.1016/j.jaerosci.2010.02.008

Middlebrook, A. M., Bahreini, R., Jimenez, J. L., & Canagaratna, M. R. (2012). Evaluation of composition-dependent collection efficiencies for the aerodyne aerosol mass spectrometer using field data. *Aerosol Science and Technology*, *46*(3), 258–271. https://doi.org/10.1080/02786826.2011.620041

Nault, B. A., Campuzano-Jost, P., Day, D. A., Guo, H., Jo, D. S., Handschy, A. V., et al. (2020). Interferences with aerosol acidity quantification due to gas-phase ammonia uptake onto acidic sulfate filter samples. *Atmospheric Measurement Techniques*, *13*(11), 6193–6213. https://doi.org/10.5194/amt-13-6193-2020

Palm, B. B., de Sá, S. S., Day, D. A., Campuzano-Jost, P., Hu, W., Seco, R., et al. (2018). Secondary organic aerosol formation from ambient air in an oxidation flow reactor in central Amazonia. *Atmospheric Chemistry and Physics*, *18*(1), 467–493. https://doi.org/10.5194/acp-18-467-2018

Saide, P. E., Gao, M., Lu, Z., Goldberg, D. L., Streets, D. G., Woo, J. H., et al. (2020). Understanding and improving model representation of aerosol optical properties for a Chinese haze event measured during KORUS-AQ. *Atmospheric Chemistry and Physics*, *20*(11), 6455–6478. https://doi.org/10.5194/acp-20-6455-2020

Salcedo, D., Onasch, T. B., Dzepina, K., Canagaratna, M. R., Zhang, Q., Huffman, J. A., et al. (2006). Characterization of ambient aerosols in Mexico city during the MCMA-2003 campaign with aerosol mass spectrometry: Results from the CENICA supersite. *Atmospheric Chemistry and Physics*, *6*(4), 925–946. https://doi.org/10.5194/acp-6-925-2006

Schroder, J. C., Campuzano-Jost, P., Day, D. A., Shah, V., Larson, K., Sommers, J. M., et al. (2018). Sources and secondary production of organic aerosols in the northeastern United States during WINTER. *Journal of Geophysical Research: Atmospheres*, *123*(14), 7771–7796. https://doi.org/10.1029/2018JD028475

Shingler, T., Crosbie, E., Ortega, A., Shiraiwa, M., Zuend, A., Beyersdorf, A., et al. (2016). Airborne characterization of subsaturated aerosol hygroscopicity and dry refractive index from the surface to 6.5 km during the SEAC4RS campaign. *Journal of Geophysical Research: Atmospheres*, *121*(8), 4188–4210. https://doi.org/10.1002/2015jd024498